Angewandte Chemie International Edition

Angewandte International Edition Chemie

How to cite: *Angew. Chem. Int. Ed.* **2026**, e5786823
doi.org/10.1002/anie.5786823

RESEARCH ARTICLE OPEN ACCESS

Iterative Synthesis of Pentacene Derivatives with Continuous Boron–Oxygen Bonds

Seonghwa Jeong[1] | Si-In Kim[1] | Jonghwan Lee[1] | Hwon Kim[1] | Jinuk Jang[1] | Jiyeon Kim[1] | Wonyoung Choe[1,2,3,4] | Seung Kyu Min[1] | Young S. Park[1]

[1]Department of Chemistry, Ulsan National Institute of Science and Technology (UNIST), Ulsan, Republic of Korea | [2]Department of Mechanical Engineering, Ulsan National Institute of Science and Technology (UNIST), Ulsan, Republic of Korea | [3]Graduate School of Carbon Neutrality, Ulsan National Institute of Science and Technology (UNIST), Ulsan, Republic of Korea | [4]Graduate School of Artificial Intelligence, Ulsan National Institute of Science and Technology (UNIST), Ulsan, Republic of Korea

Correspondence: Seung Kyu Min (skmin@unist.ac.kr) | Young S. Park (youngspark@unist.ac.kr)

Received: 5 March 2026 | **Revised:** 30 March 2026 | **Accepted:** 1 April 2026

Keywords: heterocycles | main group elements | polycycles | synthesis design

ABSTRACT

Iterative syntheses—repeating sequences of the same reactions to construct complex molecules—can facilitate the synthesis of specific classes of small molecules with structural redundancies, including acenes. Despite the prevalence of zigzag edges in the structures of acenes, few examples that effectively manipulate the edge configurations of acenes exist. In this study, the rationally designed iterative synthesis of three pentacene derivatives with continuous boron–oxygen bonds at the zigzag edges is reported. The simple and efficient two-step iteration employed *ipso* iodination with a trimethylsilyl group as the directing group and Suzuki cross-coupling/condensation reactions. Because of the fundamental role of pentacene derivatives in a broad spectrum of electronic applications, these findings are valuable across a diverse range of chemical and physical disciplines.

1 | Introduction

The development of new synthetic methodologies for organic molecules is essential for constructing new classes of materials [1, 2]. Iterative syntheses—comprising sequences of coupling and functional group generation reactions that undergo repeated cycling—can provide good accessibility to specific classes of small molecules with structural redundancies, including acenes [3–5]. Acenes are an important class of organic semiconducting molecules, with broad relevance in the domain of organic electronics [6–8]. The properties of acenes undergo substantial changes as the number of linearly fused benzene rings increases [6–13]. The molecular and electronic properties of acenes can be further modulated by incorporating heteroatoms, which induce changes in the shapes and energies of the highest occupied molecular orbital (HOMO) and/or lowest unoccupied molecular orbital (LUMO) [14–17]. The rational incorporation of heteroatoms, which is frequently challenging, is valuable for tuning the properties of carbon-based molecules (demonstrated by the successful molecular engineering of different heteroacenes to improve the performance of electronic devices) [18, 19]. Despite the prevalence of zigzag edges in the structures of acenes, few examples that exist effectively manipulate the edge configurations of acenes by introducing continuous multiple heteroatoms [20].

While the isoelectronic substitution of sp^2 hybridized carbon–carbon (CC) bonds with sp^2 hybridized boron–nitrogen (BN) bonds in π-conjugated molecules has attracted considerable attention, analogous boron–oxygen (BO) bonds remain less explored (Figure 1) [20–43]. In particular, BO bonds may provide

Seonghwa Jeong, Si-In Kim, Jonghwan Lee, and Hwon Kim contributed equally to this work.

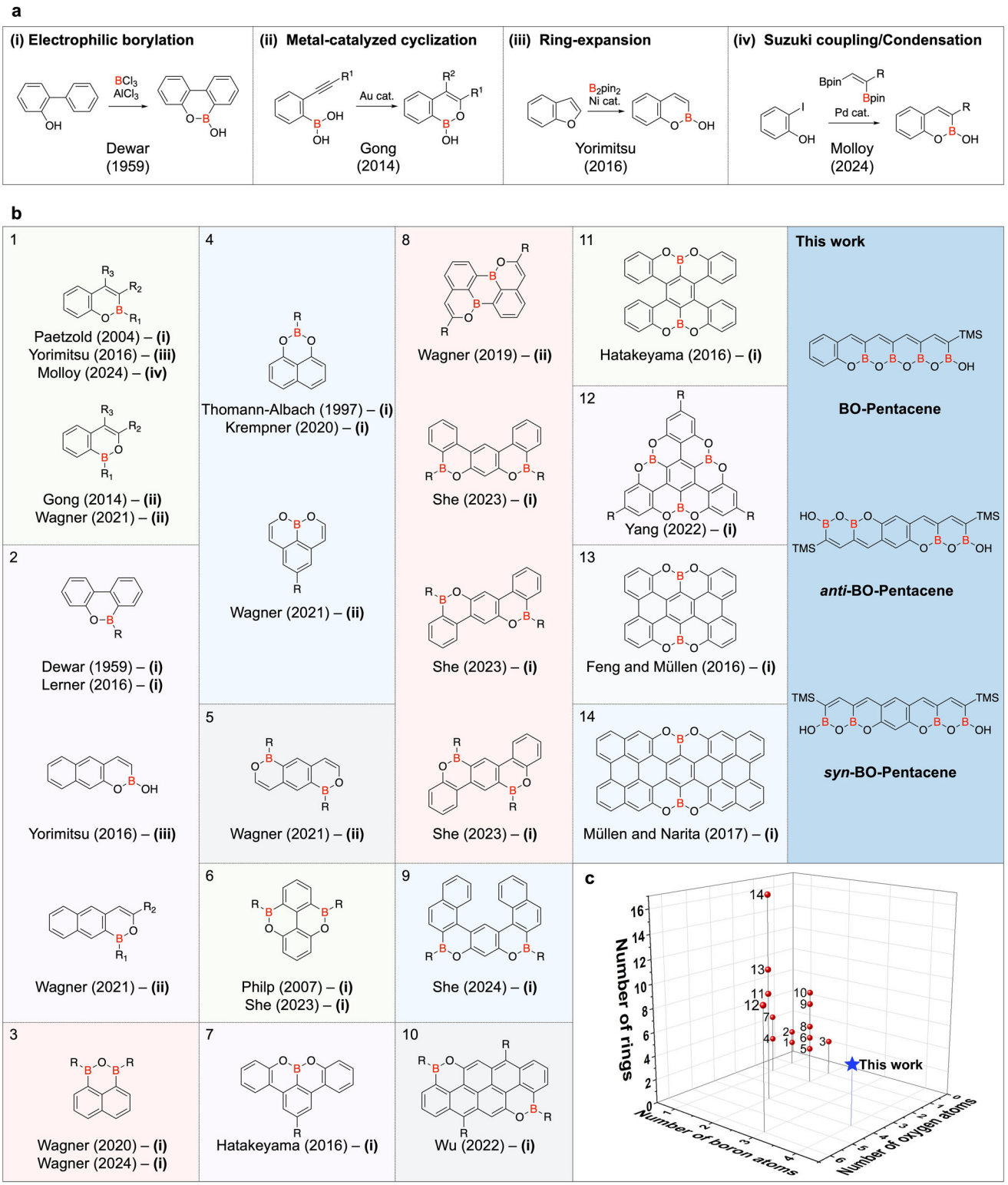

FIGURE 1 | Overview of synthetic strategies and representative structures of BO-containing molecules. (a) Representative synthetic methods for incorporating BO bonds. (b) Chemical structures of reported BO-containing benzenoids listed by increasing numbers of rings and B/O atoms. In the structures, R groups were used as substituents for clarity; refer to the original references for full details. Additionally, the research group, the year of publication, and the synthetic method utilized are appended below the chemical structures. (c) 3D scatter plot, with the number of fused rings, B atoms, and O atoms for molecules as indicated by the number in panel b. This work is denoted by a blue star.

unique characteristics because the O atom has higher electronegativity and weaker π-electron donation than the N atom. Therefore, BO bonds decrease the aromaticity of organic semiconductors [20, 21].

A limited number of synthetic methods are available for the preparation of BO-containing molecules, including electrophilic borylation, metal-catalyzed cyclization, ring-expansion, and Suzuki cross-coupling/condensation reactions (Figure 1a) [22–25]. Despite the limited number of synthetic developments, a significant number of new BO-containing benzenoid molecules have recently been prepared and studied (Figure 1b). These molecules were arranged according to their increasing number of rings and B/O atoms, with the sequence comprising at least two fused rings. In addition, the research group, year of publication, and synthetic method were also listed for these molecules. For comparison, the chemical diversities of all the molecules are also visualized in 3D space, utilizing the number of rings, B atoms, and O atoms within the molecular skeleton to highlight the relative numbers of B and O atoms with respect to the total number of fused rings (Figure 1c). Since Dewar's pioneering work on electrophilic borylation in 1959 (Figure 1a(i)) [22], the majority of BO-containing polycyclic aromatic hydrocarbons have been synthesized using this strategy, including molecules containing not only BO bonds but also OBO and BOB bonds. These structures contain molecular skeletons ranging from naphthalene (by Paetzold), phenanthrene (by Dewar and Lerner), phenalenyl (by Wagner, Thomann-Albach, and Krempner), pyrene (by Philip and She) to graphene molecules (by Hatakeyama, She, Wu, Yang, and Müllen) (Figure 1b) [22, 26–40]. In 2014, Gong and co-workers reported an Au-catalyzed cyclization (Figure 1a(ii)) [23], which was later employed by Wagner's group to synthesize BO-, OBO-, and BOB-containing naphthalenes, anthracenes, phenalenyl, and perylene derivatives (Figure 1b) [21, 41]. In 2016, Yorimitsu and co-workers reported a Ni-catalyzed ring-expansion approach (Figure 1a(iii)), which was subsequently demonstrated to be applicable to the synthesis of BO-containing naphthalene and anthracene derivatives (Figure 1b) [24]. Recently, Molloy and colleagues described a simple method for the regioselective Pd-catalyzed cross-coupling/condensation of 2-halophenols using a diboron reagent, providing valuable insights from a perspective of chemical synthesis (Figure 1a(iv)) [25].

In this study, the rationally designed iterative synthesis of three pentacene derivatives with continuous BO bonds is reported (Figure 1b, this work). Based on Molloy's synthesis, we have developed a new synthetic strategy to increase the number of continuous heteroatoms at the zigzag edges of pentacene derivatives for a significant impact on the characteristics of the molecules. One of these derivatives contains continuous BO bonds in one direction from the benzene ring (BO-pentacene), whereas the other two possess bidirectional BO bonds from the central benzene ring on the opposite side (*anti*-BO-pentacene) and on the same side (*syn*-BO-pentacene). These BO-pentacene derivatives contain a high content of heteroatoms relative to the total number of rings (Figure 1c). The prepared molecules are systematically characterized by spectroscopic techniques, electrochemical measurements, density functional theory (DFT) calculations, and X-ray crystallography. The absolute fluorescence quantum yields of all BO-pentacene derivatives are greater than 0.70. The experimental and theoretical studies suggest that the aromaticity of the BO-acene derivatives decreases when the CC bonds are replaced by BO bonds along the zigzag edge of the pentacene skeleton. Finally, the reaction mechanism is investigated both experimentally and theoretically, revealing that the Suzuki cross-coupling reaction is the origin of regioselectivity.

2 | Results and Discussion

2.1 | Development of the Proposed Synthesis Method

As a continuation of our interest in increasing the number of continuous heteroatoms at the zigzag edges of acenes, a new iterative synthetic strategy was devised. First, the viability of establishing continuous BO bonds at the zigzag edges of acene derivatives was assessed. Adapting the synthetic route for BOBN anthracene, a series of reactions, such as iodination, Suzuki cross-coupling, and BO annulation reactions (using BCl_3 instead of $PhBCl_2$ for iteration), were implemented to achieve individual yields of 75%, 57%, and 10%, respectively (Figure 2a) [20]. In principle, this facilitates the repetition of the sequence of reactions to expand the size of BO-containing acenes. However, in an iterative synthesis, performing this sequence of reactions is not effective in practical applications because of the relatively low yield of one iteration (~4%). The issue lies in the relatively low yield obtained in the borylation step. Therefore, developing efficient strategies for forming boron–carbon (BC) bonds or, more effectively, preinstalling BC bonds in vinyl reagents is vital. Accordingly, the retrosynthetic analysis was conducted based on this concept (Figure 2b). Initially, *cis*-1,2-ethylenediboronic acid or its equivalent was assumed to facilitate Suzuki cross-coupling and BO condensation in a single step. To further increase the iodination efficiency, a directing group was introduced to *cis*-1,2-ethylenediboronic acid. Consequently, the presence of two boron functional groups would enable the extension of one fused ring with the BO bond, while the trimethylsilyl (TMS) group would control the regioselectivity of the BO annulation and enhance the efficiency of the iodination. This two-step protocol is more straightforward and efficient than the three-step pathway (Figure 2a,b). Second, a tri-substituted ethene reagent functionalized with two boron units and a TMS group was prepared (Figure 2c). This two-step protocol was performed on a >60 g scale to yield diboron reagent **6** as a white solid [44–46]. Using this reagent, the regioselectivity of BO annulation was examined, and the reaction conditions were optimized by varying the base and solvent at room temperature (Figure 3a). 2-Iodophenol was allowed to react with the reagent in the presence of $Pd(dppf)Cl_2$ as the catalyst precursor (selected because of its proven efficacy in Suzuki cross-coupling reactions) [20]. This approach was regioselective and efficient. From these experiments, a maximum isolated yield of 69% (or 82%, based on nuclear magnetic resonance (NMR) spectroscopy, Figure S61) was obtained using Cs_2CO_3 as the base and tetrahydrofuran (THF)/H_2O as the solvent at room temperature (entry 1, Figure 3a). The same set of experiments was conducted using diboron reagent **5** (reported by Molloy et al.) under identical reaction conditions to compare with diboron reagent **6** [25]. The isolated yields obtained were slightly lower, ranging from 21% to 39%, due to the reaction temperature (entries 6 to 9, Figure 3a). As large acenes have poor solubility, the temperature dependence of the BO annulation

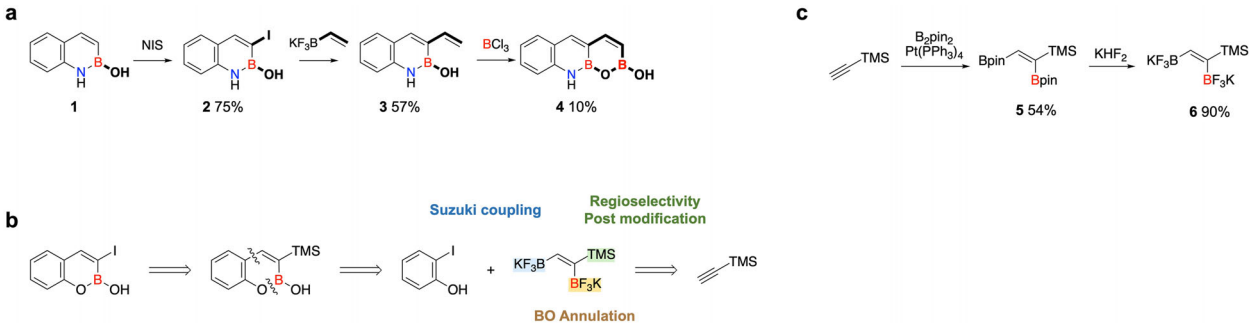

FIGURE 2 | Proposed iterative synthesis. (a) A re-examination of the BOBN anthracene synthesis, involving repeated iodination, Suzuki cross-coupling, and borylation reactions. (b) Hypothesized retrosynthetic analysis of tri-substituted diboron reagent. The diboron reagent facilitates Suzuki cross-coupling and condensation reactions, while the TMS group modulates regioselectivity and post-modification. (c) Synthesis of tri-substituted diboron reagent.

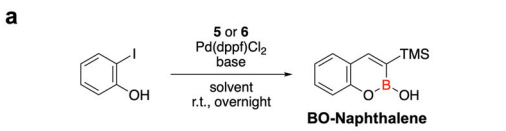

entry[a]	reagent	base	solvent	isolated yield (%)
1	**6**	**Cs_2CO_3**	**THF/H_2O**	**69 (82[b])**
2	**6**	Cs_2CO_3	MeCN/H_2O	49
3	**6**	K_3PO_4	THF/H_2O	58
4	**6**	K_3PO_4	MeCN/H_2O	27
5[c]	**6**	Cs_2CO_3	THF/H_2O	54
6	**5**	Cs_2CO_3	THF/H_2O	39
7	**5**	Cs_2CO_3	MeCN/H_2O	25
8	**5**	K_3PO_4	THF/H_2O	21
9	**5**	K_3PO_4	MeCN/H_2O	27

[a] Standard conditions: SM (0.5 mmol, 1.0 equiv.), reagent (1.5 equiv.), $Pd(dppf)Cl_2$ (0.02 equiv.), base (3.0 equiv.), solvent (2.5/2.5 mL). [b] NMR yield determined by ^1H NMR spectroscopy using 1, 3, 5-trimethoxybenzene as an internal standard. [c] $Pd(dppf)Cl_2$ (0.03 equiv.).

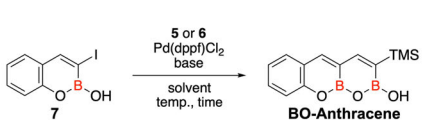

entry[a]	reagent	base	solvent	temp. (°C)	time (h)	isolated yield (%)
1	**6**	Cs_2CO_3	THF/H_2O	r.t.	overnight	58
2	**6**	Cs_2CO_3	CPME/H_2O	100	1	48
3	**6**	Cs_2CO_3	1,4-Dioxane/H_2O	100	1	49
4	**6**	Cs_2CO_3	THF/H_2O	60	1	53
5	**6**	Cs_2CO_3	MeCN/H_2O	60	1	53
6	**6**	K_3PO_4	MeCN/H_2O	60	1	46
7[b]	**6**	**Cs_2CO_3**	**THF/H_2O**	**r.t.**	**overnight**	**60 (67[c])**
8	**5**	K_3PO_4	MeCN/H_2O	60	1	45

[a] Standard conditions: SM (0.5 mmol, 1.0 equiv.), reagent (1.5 equiv.), $Pd(dppf)Cl_2$ (0.02 equiv.), base (3.0 equiv.), solvent (2.5/2.5 mL). [b] $Pd(dppf)Cl_2$ (0.03 equiv.). [c] NMR yield determined by ^1H NMR spectroscopy using 1, 3, 5-trimethoxybenzene as an internal standard.

FIGURE 3 | Reaction developments for iterative synthesis. Optimization of the Suzuki cross-coupling/condensation reaction for (a) BO-naphthalene and (b) BO-anthracene.

reaction was investigated [47]. At a higher temperature (60°C), the reaction provided slightly lower but consistent yields (44%–62%, Table S1). Third, the extension of BO-acene derivatives via iterative synthesis was attempted (Figure 3b). The two-step cycle was initiated with *ipso* iodination of the TMS group with iodine monochloride, followed by BO annulation with diboron reagent **6**. For large acenes, the reaction could be affected by molecular stability (due to the pre-existing OBO bond). Additionally, a higher temperature may be required owing to their poor solubility. Therefore, the reaction conditions for BO annulation of compound **7**, particularly the dependence on the reaction temperature and solvents, were tested. Similar to previous experiments, the reaction in different solvent mixtures provided slightly lower but consistent yields at elevated temperatures of 60–100°C (46%–53%, Figure 3b). In particular, a slightly higher yield was achieved at room temperature (58%, entry 1, Figure 3b). By modifying the equivalents of a palladium catalyst, a maximum isolated yield of 60% (or 67%, based on NMR spectroscopy, Figure S63) was obtained (entry 7, Figure 3b).

2.2 | Synthesis of BO-pentacene Derivatives by Iterative Synthesis

Next, the iterative synthesis of BO-pentacene derivatives was performed (Figure 4). This simple, yet efficient, two-step synthesis enabled the sequential linear elongation of fused rings in acene derivatives. The synthesis of BO-pentacene was accomplished in seven steps. An overall yield of 7% was achieved by unidirectional iteration using 2-iodophenol (Figure 4a). In general, BO annulation provided moderate yields (60%–69%) up to BO-tetracene, which decreased to 36% owing to the poor solubility of compound **9** (Figure 4a). Remarkably, *ipso* iodination provided considerably high isolated yields throughout the iterations (87%–91%, Figure 4a). To further illustrate the synthetic utility of this two-step iteration, diiodobenzenediols were selected as templates for bidirectional growth and compared with the unidirectional growth of BO-pentacene (Figure 4b,c). Bidirectional growth is advantageous over unidirectional growth because one iteration forms two rings, enabling rapid elongation for the construction

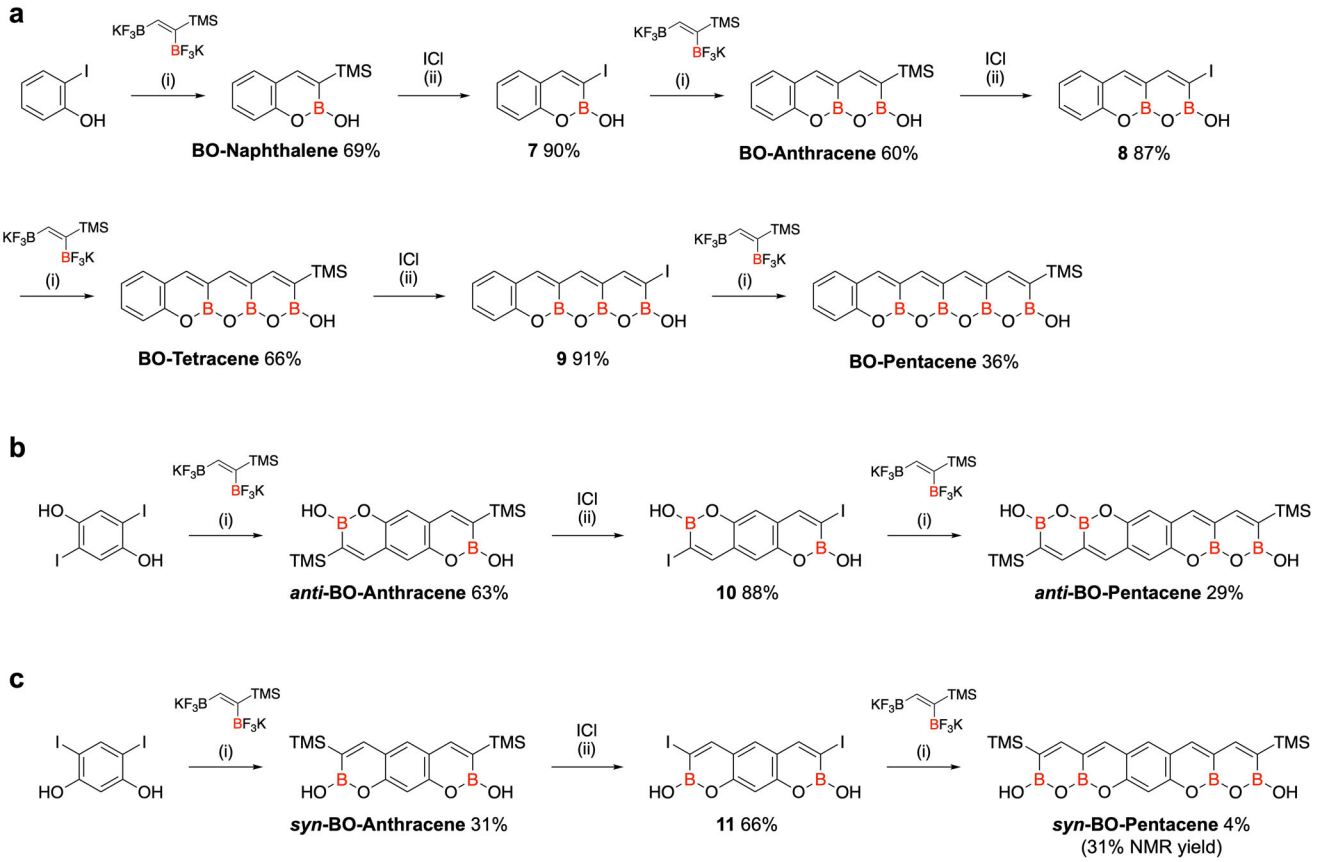

FIGURE 4 | Synthesis of BO-acenes. (a) Iterative synthesis of BO-acenes for unidirectional growth. (b) Synthesis of *anti*-BO-pentacene and (c) *syn*-BO-pentacene for bidirectional growth. Reagents and conditions: (i) $Pd(dppf)Cl_2$, Cs_2CO_3, THF/H_2O, room temperature (in Figure 4a,b) or 60°C (in Figure 4c), overnight. (ii) THF, −78°C to room temperature, 5 h.

of longer acene derivatives. Furthermore, the position of the BO bonds can be regulated by the structures of diiodobenzenediols in either *anti*- or *syn*-geometry. In these configurations, the zigzag edges of the acene derivatives contained BO bonds in either *anti*- or *syn*-like structures (i.e., BO bonds on the opposite side or BO bonds on the same side, respectively). To prepare *anti*- and *syn*-BO-anthracene, diboron reagent **6** was reacted with 2,5-diiodobenzene-1,4-diol and 4,6-diiodobenzene-1,3-diol, respectively, under optimal conditions (conditions (i) shown in Figure 4b,c); the isolated yields of *anti*- and *syn*-BO-anthracene were 63% and 31%, respectively. Then, the two TMS groups in *anti*- and *syn*-BO-anthracene were converted to two iodide groups by *ipso* iodination (compounds **10** and **11**), considering the subsequent iteration; the isolated yields of compounds **10** and **11** were 88% and 66%, respectively. Subsequently, *anti*- and *syn*-BO-pentacene were obtained from compounds **10** and **11**, respectively, under the optimal conditions. For *syn*-BO-pentacene, the reaction temperature was increased to 60°C due to the slightly lower reactivity of compound **11**. The decreased stability of *syn*-BO-pentacene resulted in a low isolated yield of 4%, despite the 31% yield determined by NMR spectroscopy, suggesting that decomposition had occurred during the purification process (Figure S64). Overall, *anti*-BO-pentacene and *syn*-BO-pentacene were synthesized in three steps by bidirectional iteration with overall yields of 16% and 1%, respectively. The structures of BO-pentacene derivatives were thoroughly analyzed using ^{1}H, ^{13}C, and ^{11}B NMR spectroscopy and mass spectrometry (Supporting Information).

Then, a crystal of BO-pentacene was grown by vapor diffusion in THF and diethyl ether; its solid-state structure was analyzed using single-crystal X-ray diffraction (Figure 5 and Table S2) [48]. The crystal structure of BO-pentacene confirmed that the iterative synthesis produced the desired structure (further supported by the detailed NMR analysis of BO-pentacene (Figures S37–S39)). In particular, the BO bond length in the ring structure was almost constant (1.37–1.39 Å), while the CC bond length at the opposite edge was alternating yet constant between the conjugated single bond (1.43–1.45 Å) and double bond (1.35–1.36 Å) (Figure S1). Therefore, the incorporation of a continuous BO bond at the zigzag edge of the opposite side decreased the delocalization of π-electrons throughout the pentacene core. The overall lengths of the CC bonds were greater than those of the BO bonds, resulting in a slight convex curvature at the zigzag edge of the carbon atoms (Figure 5a). Distinctive variations between the BO and BN bonds in acenes were observed by comparing BO-pentacene and BNBN anthracene [20]. In accordance with previous reports, the bond lengths of BO in BO-pentacene were significantly shorter than those of BN in BNBN anthracene (1.41–1.44 Å) [20, 21]. The CC bonds at the opposite edge indicated the same bond length alternation, with similar bond lengths for both BO-pentacene and BNBN anthracene [20]. The average bond angle of the B—O—B moiety in BO-pentacene was approximately 119.3°, while that of the B–N–B unit in BNBN anthracene was 122.4°, indicating subtle changes between the O and N atoms. The crystal structure of BO-pentacene also revealed an almost planar geometry of the pentacene scaffold with a

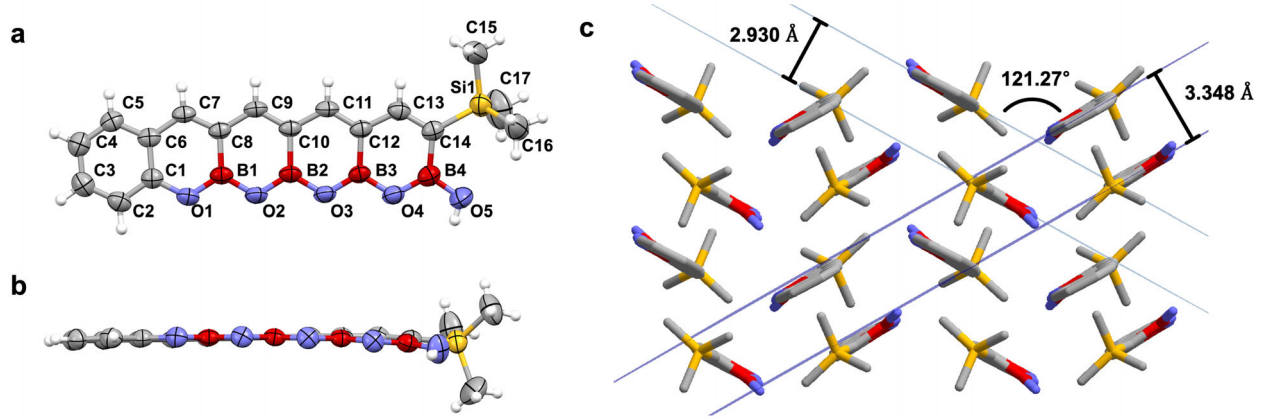

FIGURE 5 | Single-crystal structure of BO-pentacene. (a) Top view. (b) Side view along the B2—C10 direction. Displacement ellipsoids are shown at the 50% probability level. (c) γ-Type packing structure with intermolecular distances of 2.930 and 3.348 Å, and an interplanar angle of 121.27°. Carbon, oxygen, boron, silicon, and hydrogen atoms are shown in gray, purple, red, yellow, and white, respectively.

sagging corner of the B atom, which could be attributed to the steric hindrance from the bulky TMS group (Figure 5b). In the crystal packing, the BO-pentacene molecules adopted a face-to-face alignment with opposite orientations (Figure 5c). This was a typical characteristic of a γ-structure, in which the conjugated molecular planes stacked parallel to each other, facilitating strong π–π interactions. Structural analysis revealed intermolecular distances of 2.930 and 3.348 Å, with an angle of 121.27° between the mean planes of neighboring molecules (Figure 5c). This face-to-face arrangement contrasted with the conventional herringbone packing in pentacene, where the molecules adopted an edge-to-face configuration [49, 50]. Such molecular arrangement in BO-pentacene could promote intermolecular electronic coupling.

2.3 | Molecular Properties of BO-pentacene Derivatives

Next, BO-pentacene derivatives were characterized using ultraviolet–visible (UV/Vis) spectroscopy (left, Figure 6a). The absorbance spectra of *anti*- and *syn*-BO-pentacene showed strong, well-resolved maximum peaks. Clusters of the characteristic absorption peaks were observed at 363, 383, and 404 nm for *anti*-BO-pentacene and at 366 and 385 nm for *syn*-BO-pentacene. In comparison, the spectrum of BO-pentacene was broad, with absorption peaks at 404 and 423 nm. Based on the absorption onsets, the optical HOMO–LUMO energy gaps (E_g^{opt}s) for BO-pentacene, *anti*-BO-pentacene, and *syn*-BO-pentacene were 2.60, 3.00, and 3.12 eV, respectively. These molecules were then analyzed using fluorescence spectroscopy (right, Figure 6a). The emission spectra obtained for *anti*- and *syn*-BO-pentacene exhibited similar shapes, with sharp bands and Stokes shifts of 1920 and 1990 cm^{-1}, respectively. The emission spectra of BO-pentacene exhibited a broad signal (as observed in the absorbance spectra) with a large Stokes shift of 4300 cm^{-1}. The absolute fluorescence quantum yields were high and determined as 0.73, 0.70, and 0.75 for BO-pentacene, *anti*-BO-pentacene, and *syn*-BO-pentacene, respectively (Table 1).

Subsequently, the electrochemical behavior of the BO-pentacene derivatives was investigated using cyclic voltammetry (Figure S5 and Table 1). Reversible redox couples were not observed in the voltammograms of the molecules. For BO-pentacene, the voltammogram exhibited onsets of reduction and oxidation potentials at –1.22 and 0.89 V vs. ferrocene/ferrocenium (Fc/Fc^+), respectively. For *anti*-BO-pentacene and *syn*-BO-pentacene, these potentials were observed at –1.26 and 1.04 V vs. Fc/Fc^+ and –1.34 and 1.00 V vs. Fc/Fc^+, respectively. The electrochemical HOMO–LUMO energy gaps (E_g^{el}s) for BO-pentacene, *anti*-BO-pentacene, and *syn*-BO-pentacene were 2.11, 2.30, and 2.34 eV, respectively, based on their onset potentials. In general, the trends in the estimated E_g^{el}s were similar to those of E_g^{opt}s.

The electronic structures and chemical bonds composed of multiple BO bonds in different geometries were further analyzed by performing DFT calculations for the BO-pentacene derivatives (computational details are provided in the Supporting Information). We optimized the geometries of the molecules using the B3LYP functional and the 6-31G(d) basis, with the solvent effect accounted for using the polarizable continuum model in the integral equation formalism variant. Dichloromethane was used as the solvent to match the experimental conditions. The structural features of the B—O, C—O, C—C, and C=C bond lengths of BO-pentacene were in agreement with the experimental values (Figure S67). Figure 6b shows the shapes and energies of the frontier molecular orbitals, including the E_gs of BO-pentacene derivatives. Upon the introduction of continuous BO bonds to the zigzag edges of the pentacene skeleton, the shapes of the HOMOs and LUMOs of the BO-pentacene derivatives were significantly affected by the positions of the BO bonds. In particular, in all cases, the electron densities were predominantly located along the C=C—B bond in the HOMOs and along the C—C—B bond in the LUMOs. Although the O atoms show sp^2 hybridization with planar structures for all compounds, the DFT calculations indicated that the electron densities on the O atoms were negligible in both HOMOs and LUMOs in all cases due to the large electronegativity difference between the O and C atoms, except for the HOMO of *syn*-BO-pentacene. The electron density on the O atoms provided additional stabilization, which lowered the HOMO energy of *syn*-BO-pentacene. Figure 6b shows that the trends observed in the energies of the HOMO, LUMO, and E_g of the BO-pentacene derivatives are similar to those of the experimental results. In general, the E_gs of the BO-pentacene derivatives increased from BO-pentacene to *anti*-BO-pentacene

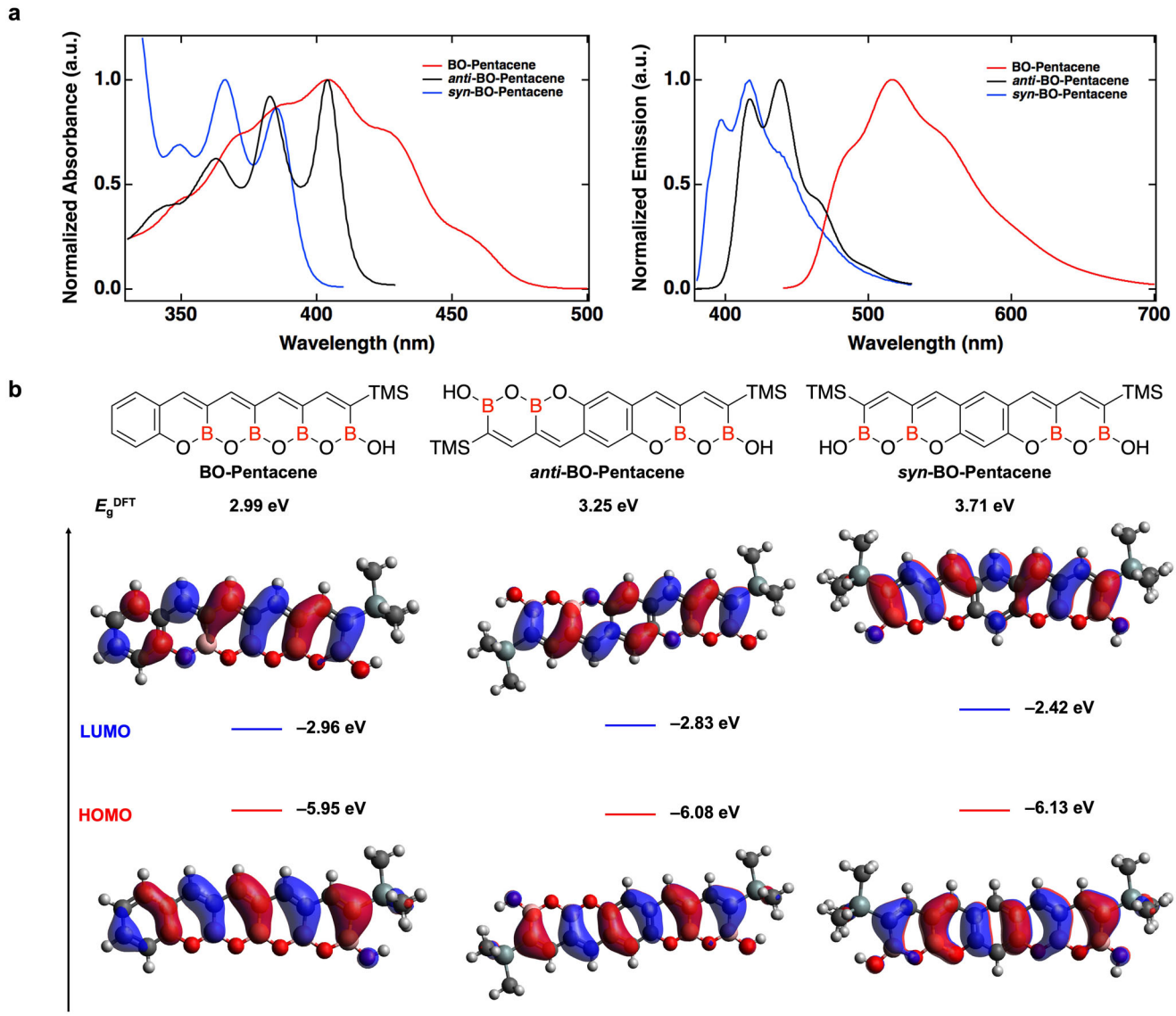

FIGURE 6 | Optical properties and DFT calculations of BO-pentacene derivatives. (a) UV/Vis absorbance and emission spectra of BO-pentacene (red), *anti*-BO-pentacene (black), and *syn*-BO-pentacene (blue) in dichloromethane (1.0×10^{-5} M). The excitation wavelengths for the emission spectra were 404, 404, and 385 nm, respectively. (b) Frontier molecular orbitals and their energies of BO-pentacene, *anti*-BO-pentacene, and *syn*-BO-pentacene. Values were calculated using the B3LYP functional and 6-31G(d) basis.

TABLE 1 | Optical and electrochemical properties of BO-pentacene derivatives.

Compound	λ_{abs} [nm]	λ_{em}[a] [nm]	ϕ[b]	HOMO[c] [eV]	LUMO[c] [eV]	E_g^{opt}[d] [E_g[e]] [eV]	Stokes shift[f] [cm^{-1}]
BO-Pentacene	423	517	0.73	−5.69	−3.58	2.60 [2.11]	4300
anti-BO-Pentacene	404	438	0.70	−5.84	−3.54	3.00 [2.30]	1920
syn-BO-Pentacene	385	417	0.75	−5.80	−3.46	3.12 [2.34]	1990

[a]Excited at 404 nm (BO-pentacene and *anti*-BO-pentacene) and 385 nm (*syn*-BO-pentacene).
[b]Determined using the integrating sphere method in dichloromethane.
[c]Determined from the onset potential of the redox couple observed by cyclic voltammetry, with ferrocene as the external standard. HOMO $=-(E_{ox/onset} + 4.80)$ eV. LUMO $=-(E_{red/onset} + 4.80)$ eV.
[d]Optical HOMO–LUMO energy gap. Determined from the absorption onset in the UV/Vis spectrum.
[e]Electrochemical HOMO–LUMO energy gap.
[f]Determined from λ_{abs} and λ_{em} in Table 1.

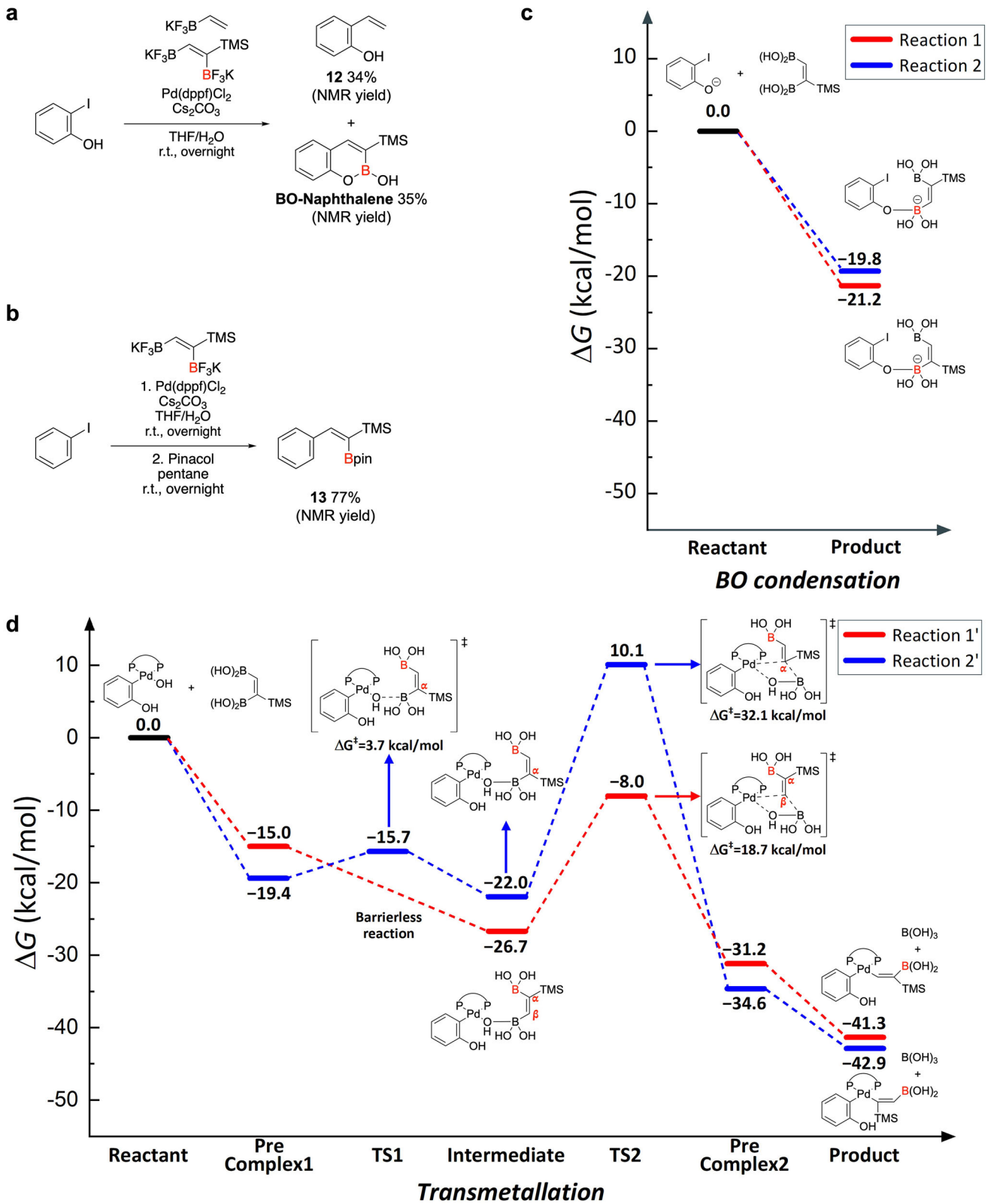

FIGURE 7 | Experimental and computational investigation of regioselectivity. (a) Competition experiment. (b) Evaluation of regioselectivity in the absence of the OH group. (c) Gibbs free energy diagram for the BO condensation reaction. (d) Gibbs free energy diagram for the transmetallation step in the Suzuki cross-coupling.

to *syn*-BO-pentacene, which was in good agreement with E_g^{opt}s and E_g^{el}s from experiments. In addition, the HOMO to LUMO transition was dominant for the first absorption peak (Table S5 and Figure S69). Furthermore, nucleus-independent chemical shift (NICS) calculations confirmed that the aromaticity of the BO-pentacene derivatives decreased when the CC bonds were replaced, thereby forming BO bonds along the zigzag edge of the pentacene skeleton (Figure S68).

2.4 | Regioselectivity in BO Annulation

To elucidate the origin of regioselectivity, a series of controlled experiments were carried out. Assuming the condensation reaction is relatively faster than the Suzuki cross-coupling, the competition experiment involving boron reagents and 2-iodophenol was conducted (Figure 7a). To facilitate the regioselective reaction, the condensation reaction must occur selectively between the internal boron group and hydroxy group. Subsequently, the intramolecular Suzuki cross-coupling reaction should occur. This hypothesized reaction pathway is expected to result in the regioselective formation of BO-naphthalene. Consequently, the expectation was that the conversion yield from the diboron reagent **6** would exceed that from the use of potassium vinyltrifluoroborate. Notably, the conversion yield obtained from the use of two boron reagents was comparable. Subsequently, iodobenzene was subjected to a reaction with diboron reagent **6** (Figure 7b). As reported in a previous study, the terminal boron group exhibited a selective reaction over the internal boron group, yielding the regioselective product **13** [51]. These findings suggest that the Suzuki cross-coupling is the mechanistic basis for the observed regioselectivity.

To elucidate the theoretical basis underlying the regioselectivity observed in the synthesis of BO-acene derivatives, DFT calculations were carried out to uncover the mechanistic details of the condensation reaction and transmetallation step in Suzuki cross-coupling (Figure 7c,d). We evaluated two possible condensation pathways with different regioisomers (Reaction 1 and 2 in Figure 7c). The calculations indicate that both are exergonic and proceed without any well-defined transition state (TS). Moreover, these two pathways are energetically competitive, suggesting that the condensation reaction is not the primary factor determining regioselectivity. Regarding the transmetallation step in Suzuki cross-coupling, previous studies have proposed two plausible mechanisms: the boronate pathway and oxo-palladium pathway [52]. The latter is now widely accepted due to the experimental evidence demonstrating that Pd–OH species typically react with boronic acids more rapidly than preformed boronates. Consistent with these findings, our computational results show that the compounds associated with the oxo-palladium pathway are thermodynamically more stable than those in the boronate pathway by 12.9 kcal/mol. Building on this insight, we examined two potential transmetallation scenarios: β-carbon functionalization relative to the TMS group (Reaction 1' via the terminal boron group) and α-carbon functionalization (Reaction 2' via the internal boron group). The calculated Gibbs free energy profiles indicate that both reaction pathways are exergonic and therefore thermodynamically favorable (Figure 7d). However, their kinetic features differ significantly. For the initial approach of the oxygen to the boron center (from pre-complex 1 to intermediate), the minimum energy pathway of Reaction 1', obtained via the nudge elastic band method, shows a continuous decrease in energy, indicating a barrierless process (Figure S70). Conversely, Reaction 2' requires an activation energy of 3.7 kcal/mol, featuring the TS structure with a B—O distance of 2.22 Å, a structural midpoint between the 2.80 Å found in pre-complex 1 and 2.16 Å of the intermediate. Moreover, the subsequent step involving Pd—C bond formation and Pd—O bond cleavage (from intermediate to pre-complex 2) revealed an even more significant kinetic discrepancy. Reaction 2' exhibited a substantial reaction barrier of 32.1 kcal/mol, whereas Reaction 1' proceeded with a much lower barrier of 18.7 kcal/mol. This significant difference in activation energy (13.4 kcal/mol) clearly indicates that the regioselectivity is governed by the kinetics in the transmetallation in Suzuki cross-coupling, favoring Reaction 1' in excellent agreement with experimental observations.

Overall, the condensation reaction would be fast in equilibrium, and the transmetallation step in the Suzuki cross-coupling reaction is the rate-determining step, which controls the regioselectivity of the reaction.

3 | Conclusion

An iterative strategy for the synthesis of three BO-pentacene derivatives, a new class of π-conjugated molecules with continuous BO bonds, was developed. The two-step iterative process (executed in a unidirectional or bidirectional manner) introduced continuous BO bonds at the zigzag edges of the pentacene moiety in three distinct modes. In this approach, a TMS group was introduced as a directing group for the introduction of iodide, which was effective as it significantly increased the yield compared to that of a standard iodination reaction that did not involve a directing group. Based on Molloy's synthesis, the Suzuki cross-coupling and BO condensation reactions were employed to form BO-containing six-membered rings in one step. This efficient two-step protocol comprised one cycle of iterations, after which the molecule could be used in another cycle. In particular, our scalable approach employed an iterative process under straightforward reaction conditions. These advantages facilitated the preparation of BO-containing acene derivatives with variable lengths of acene and varying positions of the continuous BO bonds at the zigzag edge. This approach enabled the expansion of the chemical diversity of acenes and a more comprehensive analysis of the effects of the BO units in acenes. Moreover, BO-acenes could serve as precursors for BN-acenes via oxygen–nitrogen exchange reactions. Therefore, the findings of this study open new research avenues and provide unique opportunities for the synthesis of acene-based functional materials for application in optoelectronic semiconductor devices.

Acknowledgments

This work was supported by a National Research Foundation of Korea (NRF) grant funded by the Korean Government (RS-2024-00356302 (Y.P.), RS-2023-00257666 (S.M.), RS-2024-00455131 (S.M.), RS-2025-00513741 (W.C.)), Institute of Information & Communications Technology Planning & Evaluation (IITP) grant funded by the Korea government (MSIT) (RS-2020-II201336 (W.C.)). This study contains the results obtained by using the equipment of UNIST Central Research Facilities (UCRF).

Conflicts of Interest

The authors declare no conflicts of interest.

Data Availability Statement

The data that support the findings of this study are available from the corresponding author upon reasonable request.

References

1. M. Stępień, E. Gońka, M. Żyła, and N. Sprutta, "Heterocyclic Nanographenes and Other Polycyclic Heteroaromatic Compounds: Synthetic Routes, Properties, and Applications," *Chemical Reviews* 117 (2017): 3479–3716.

2. A. Borissov, Y. K. Maurya, L. Moshniaha, W.-S. Wong, M. Żyła-Karwowska, and M. Stępień, "Recent Advances in Heterocyclic Nanographenes and Other Polycyclic Heteroaromatic Compounds," *Chemical Reviews* 122 (2022): 565–788, https://doi.org/10.1021/acs.chemrev.1c00449.

3. J. W. Lehmann, D. J. Blair, and M. D. Burke, "Towards the Generalized Iterative Synthesis of Small Molecules," *Natural Chemical Review* 2 (2018): 0115, https://doi.org/10.1038/s41570-018-0115.

4. R. Obexer, M. Nassir, E. R. Moody, P. S. Baran, and S. L. Lovelock, "Modern Approaches to Therapeutic Oligonucleotide Manufacturing," *Science* 384 (2024): eadl4015, https://doi.org/10.1126/science.adl4015.

5. K. Molga, S. Szymkuć, P. Gołębiowska, et al., "A Computer Algorithm to Discover Iterative Sequences of Organic Reactions," *Nature Synthesis* 1 (2022): 49–58, https://doi.org/10.1038/s44160-021-00010-3.

6. J.-L. Brédas, D. Beljonne, V. Coropceanu, and J. Cornil, "Charge-Transfer and Energy-Transfer Processes in π-Conjugated Oligomers and Polymers: A Molecular Picture," *Chemical Reviews* 104 (2004): 4971–5004.

7. J. E. Anthony, "The Larger Acenes: Versatile Organic Semiconductors," *Angewandte Chemie International Edition* 47 (2008): 452–483, https://doi.org/10.1002/anie.200604045.

8. M. Watanabe, K.-Y. Chen, Y. J. Chang, and T. J. Chow, "Acenes Generated From Precursors and Their Semiconducting Properties," *Accounts of Chemical Research* 46 (2013): 1606–1615, https://doi.org/10.1021/ar400002y.

9. M. Bendikov, H. M. Duong, K. Starkey, K. N. Houk, E. A. Carter, and F. Wudl, "Oligoacenes: Theoretical Prediction of Open-Shell Singlet Diradical Ground States," *Journal of the American Chemical Society* 126 (2004): 7416–7417, https://doi.org/10.1021/ja048919w.

10. R. Mondal, B. K. Shah, and D. C. Neckers, "Photogeneration of Heptacene in a Polymer Matrix," *Journal of the American Chemical Society* 128 (2006): 9612–9613, https://doi.org/10.1021/ja063823i.

11. R. Mondal, C. Tönshoff, D. Khon, D. C. Neckers, and H. F. Bettinger, "Synthesis, Stability, and Photochemistry of Pentacene, Hexacene, and Heptacene: A Matrix Isolation Study," *Journal of the American Chemical Society* 131 (2009): 14281–14289, https://doi.org/10.1021/ja901841c.

12. C. Tönshoff and H. F. Bettinger, "Photogeneration of Octacene and Nonacene," *Angewandte Chemie International Edition* 49 (2010): 4125–4128, https://doi.org/10.1002/anie.200906355.

13. T. Kitao, T. Miura, R. Nakayama, et al., "Synthesis of Polyacene by Using a Metal–organic Framework," *Nature Synthesis* 2 (2023): 848–854, https://doi.org/10.1038/s44160-023-00310-w.

14. U. H. F. Bunz, "The Larger Linear N-Heteroacenes," *Accounts of Chemical Research* 48 (2015): 1676–1686, https://doi.org/10.1021/acs.accounts.5b00118.

15. U. H. F. Bunz and J. Freudenberg, "*N*-Heteroacenes and *N*-Heteroarenes as *N*-Nanocarbon Segments," *Accounts of Chemical Research* 52 (2019): 1575–1587, https://doi.org/10.1021/acs.accounts.9b00160.

16. S. Dong, T. Y. Gopalakrishna, Y. Han, et al., "Extended Bis(anthraoxa)Quinodimethanes With Nine and Ten Consecutively Fused Six-Membered Rings: Neutral Diradicaloids and Charged Diradical Dianions/Dications," *Journal of the American Chemical Society* 141 (2019): 62–66, https://doi.org/10.1021/jacs.8b10279.

17. C. Chen, Y. Guo, Z. Chang, K. Müllen, and X.-Y. Wang, "Synthesis of Quadruply Boron-doped Acenes With Stimuli-responsive Multicolor Emission," *Nature Communications* 15 (2024): 8555, https://doi.org/10.1038/s41467-024-51806-8.

18. J. E. Anthony, "Functionalized Acenes and Heteroacenes for Organic Electronics," *Chemical Reviews* 106 (2006): 5028–5048, https://doi.org/10.1021/cr050966z.

19. W. Jiang, Y. Li, and Z. Wang, "Heteroarenes as High Performance Organic Semiconductors," *Chemical Society Reviews* 42 (2013): 6113, https://doi.org/10.1039/c3cs60108k.

20. S. Jeong, E. Park, J. Kim, et al., "Increasing Chemical Diversity of B_2N_2 Anthracene Derivatives by Introducing Continuous Multiple Boron-Nitrogen Units," *Angewandte Chemie International Edition* 62 (2023): e202314148, https://doi.org/10.1002/anie.202314148.

21. O. Ouadoudi, T. Kaehler, M. Bolte, H.-W. Lerner, and M. Wagner, "One Tool to Bring Them All: Au-catalyzed Synthesis of B,O- and B,N-doped PAHs From Boronic and Borinic Acids," *Chemical Science* 12 (2021): 5898–5909, https://doi.org/10.1039/D1SC00543J.

22. M. J. S. Dewar and R. Dietz, "Aromatic Boron-oxygen Heterocycles," *Tetrahedron Letters* 1 (1959): 21–23, https://doi.org/10.1016/S0040-4039(01)99449-3.

23. R. Guo, K.-N. Li, B. Liu, H.-J. Zhu, Y.-M. Fan, and L.-Z. Gong, "Asymmetric Synthesis of Heteroaryl Atropisomers via a Gold-catalyzed Cycloisomerization–amination Cascade Reaction," *Chemical Communications* 50 (2014): 5451–5454, https://doi.org/10.1039/C4CC01397B.

24. H. Saito, S. Otsuka, K. Nogi, and H. Yorimitsu, "Nickel-Catalyzed Boron Insertion Into the C2–O Bond of Benzofurans," *Journal of the American Chemical Society* 138 (2016): 15315–15318, https://doi.org/10.1021/jacs.6b10255.

25. A. Marotta, H. M. Kortman, C. Interdonato, P. H. Seeberger, and J. J. Molloy, "Convergent Synthesis of Bicyclic Boronates via a Cascade Regioselective Suzuki–Miyaura/Cyclisation Protocol," *Chemical Communications* 60 (2024): 13223–13226, https://doi.org/10.1039/D4CC04653F.

26. P. Paetzold, C. Stanescu, J. R. Stubenrauch, M. Bienmüller, and U. Englert, "1-Azonia-2-boratanaphthalenes," *Zeitschrift Für Anorganische und Allgemeine Chemie* 630 (2004): 2632–2640, https://doi.org/10.1002/zaac.200400333.

27. A. Budanow, E. von Grotthuss, M. Bolte, M. Wagner, and H.-W. Lerner, "10,9-Oxaboraphenanthrenes as Luminescent Fluorophores," *Tetrahedron* 72 (2016): 1477–1484, https://doi.org/10.1016/j.tet.2016.01.054.

28. A. S. Scholz, J. G. Massoth, M. Bursch, et al., "BNB-Doped Phenalenyls: Modular Synthesis, Optoelectronic Properties, and One-Electron Reduction," *Journal of the American Chemical Society* 142 (2020): 11072–11083, https://doi.org/10.1021/jacs.0c03118.

29. A. S. Scholz, M. Bolte, A. Virovets, et al., "Tetramerization of BEB-Doped Phenalenyls to Obtain $(BE)_8$-[16]Annulenes (E = N, O)," *Journal of the American Chemical Society* 146 (2024): 12100–12112, https://doi.org/10.1021/jacs.4c02163.

30. A. Lang, H. Nöth, and M. Thomann-Albach, "Contributions of the Chemistry of Boron, 236. In Quest of New and Stable Bis(organyloxy)Boranes $(RO)_2BH$ for Catalytic Hydroboration," *Chemische Berichte* 130 (1997): 363–370, https://doi.org/10.1002/cber.19971300310.

31. C. P. Manankandayalage, D. K. Unruh, and C. Krempner, "Boronic, Diboronic and Boric Acid Esters of 1,8-naphthalenediol—synthesis, Structure and Formation of Boronium Salts," *Dalton Transactions* 49 (2020): 4834–4842, https://doi.org/10.1039/D0DT00745E.

32. M. Numano, N. Nagami, S. Nakatsuka, et al., "Synthesis of Boronate-Based Benzo[*fg*]Tetracene and Benzo[*hi*]Hexacene via Demethylative Direct Borylation," *Chemical European Journal* 22 (2016): 11574–11577, https://doi.org/10.1002/chem.201602753.

33. L. M. Greig, A. M. Z. Slawin, M. H. Smith, and D. Philp, "The Dynamic Covalent Chemistry of Mono- and Bifunctional Boroxoaromatics," *Tetrahedron* 63 (2007): 2391–2403, https://doi.org/10.1016/j.tet.2006.12.034.

34. G. Li, K. Xu, J. Zheng, et al., "Double Boron–oxygen-fused Polycyclic Aromatic Hydrocarbons: Skeletal Editing and Applications as Organic Optoelectronic Materials," *Nature Communications* 14 (2023): 7089, https://doi.org/10.1038/s41467-023-42973-1.

35. G. Li, K. Xu, J. Zheng, et al., "High-Performance Ultraviolet Organic Light-Emitting Diodes Enabled by Double Boron–Oxygen-Embedded Benzo[*m*]Tetraphene Emitters," *Journal of the American Chemical Society* 146 (2024): 1667–1680, https://doi.org/10.1021/jacs.3c12517.

36. Y. Gu, R. Muñoz-Mármol, W. Fan, et al., "Peri-Acenoacene for Solution Processed Distributed Feedback Laser: The Effect of 1,2-Oxaborine Doping," *Advanced Optical Materials* 10 (2022): 2102782, https://doi.org/10.1002/adom.202102782.

37. T. Katayama, S. Nakatsuka, H. Hirai, et al., "Two-Step Synthesis of Boron-Fused Double Helicenes," *Journal of the American Chemical Society* 138 (2016): 5210–5213, https://doi.org/10.1021/jacs.6b01674.

38. X.-Y. Wang, A. Narita, W. Zhang, X. Feng, and K. Müllen, "Synthesis of Stable Nanographenes With OBO-Doped Zigzag Edges Based on Tandem Demethylation-Electrophilic Borylation," *Journal of the American Chemical Society* 138 (2016): 9021–9024, https://doi.org/10.1021/jacs.6b04092.

39. X.-Y. Wang, T. Dienel, M. Di Giovannantonio, et al., "Heteroatom-Doped Perihexacene From a Double Helicene Precursor: On-Surface Synthesis and Properties," *Journal of the American Chemical Society* 139 (2017): 4671–4674, https://doi.org/10.1021/jacs.7b02258.

40. X. Chen, D. Tan, J. Dong, T. Ma, Y. Duan, and D.-T. Yang, "[4]Triangulenes Modified by Three Oxygen-Boron-Oxygen (OBO) Units: Synthesis, Characterizations, and Anti-Kasha Emissions," *Journal of Physical Chemistry Letters* 13 (2022): 10085–10091, https://doi.org/10.1021/acs.jpclett.2c02986.

41. T. Kaehler, M. Bolte, H.-W. Lerner, and M. Wagner, "Introducing Perylene as a New Member to the Azaborine Family," *Angewandte Chemie International Edition* 58 (2019): 11379–11384, https://doi.org/10.1002/anie.201905823.

42. P. G. Campbell, A. J. V. Marwitz, and S.-Y. Liu, "Recent Advances in Azaborine Chemistry," *Angewandte Chemie International Edition* 51 (2012): 6074–6092, https://doi.org/10.1002/anie.201200063.

43. Z. X. Giustra and S.-Y. Liu, "The State of the Art in Azaborine Chemistry: New Synthetic Methods and Applications," *Journal of the American Chemical Society* 140 (2018): 1184–1194, https://doi.org/10.1021/jacs.7b09446.

44. T. Ishiyama, N. Matsuda, N. Miyaura, and A. Suzuki, "Platinum(0)-catalyzed Diboration of Alkynes," *Journal of the American Chemical Society* 115 (1993): 11018–11019, https://doi.org/10.1021/ja00076a081.

45. J. Ramírez and E. Fernandez, "Convenient Synthesis of α,α-Difluorinated Carbonyl Compounds From Alkynes Through a Fluorodeboronation Process," *Synthesis* 10 (2005): 1698–1700.

46. S. Darses and J.-P. Genet, "Potassium Organotrifluoroborates: New Perspectives in Organic Synthesis," *Chemical Reviews* 108 (2008): 288–325, https://doi.org/10.1021/cr0509758.

47. L. Lerena, R. Zuzak, S. Godlewski, and A. M. Echavarren, "The Journey for the Synthesis of Large Acenes," *Chemical European Journal* 30 (2024): e202402122, https://doi.org/10.1002/chem.202402122.

48. Deposition number 2427506 (for BO-Pentacene) contain the supplementary crystallographic data for this paper These data are provided free of charge by the joint Cambridge Crystallographic Data Centre and Fachinformationszentrum Karlsruhe Access Structures service.

49. R. B. Campbell, J. M. Robertson, and J. Trotter, "The Crystal Structure of Hexacene, and a Revision of the Crystallographic Data for Tetracene," *Acta Crystallographica* 15 (1962): 289–290, https://doi.org/10.1107/S0365110X62000699.

50. D. Holmes, S. Kumaraswamy, A. J. Matzger, and K. P. C. Vollhardt, "On the Nature of Nonplanarity in the [N]Phenylenes," *Chemical European Journal* 5 (1999): 3399–3412, https://doi.org/10.1002/(SICI)1521-3765(19991105)5:11%3c3399::AID-CHEM3399%3e3.0.CO;2-V.

51. N. Iwadate and M. Suginome, "Differentially Protected Diboron for Regioselective Diboration of Alkynes: Internal-Selective Cross-Coupling of 1-Alkene-1,2-diboronic Acid Derivatives," *Journal of the American Chemical Society* 132 (2010): 2548–2549, https://doi.org/10.1021/ja1000642.

52. A. J. J. Lennox and G. C. Lloyd-Jones, "Transmetalation in the Suzuki–Miyaura Coupling: The Fork in the Trail," *Angewandte Chemie International Edition* 52 (2013): 7362–7370, https://doi.org/10.1002/anie.201301737.

Supporting Information

Additional supporting information can be found online in the Supporting Information section.

The authors have cited additional references

within the Supporting Information [53–78].

Supporting File 1: anie72199-sup-0001-SuppMat.docx.